Eur. Phys. J. C (2016) 76:454
DOI 10.1140/epjc/s10052-016-4306-3

THE EUROPEAN PHYSICAL JOURNAL C

CrossMark

Regular Article - Theoretical Physics

D-wave charmonia $\eta_{c2}(1^1D_2)$, $\psi_2(1^3D_2)$, and $\psi_3(1^3D_3)$ in B_c decays

Qiang Li[a], **Tianhong Wang**[b], **Yue Jiang**[c], **Han Yuan**[d], **Guo-Li Wang**[e]

Department of Physics, Harbin Institute of Technology, Harbin 150001, People's Republic of China

Received: 11 July 2016 / Accepted: 1 August 2016 / Published online: 12 August 2016

Abstract We study the semileptonic and nonleptonic decays of B_c meson to D-wave charmonia, namely, $\eta_{c2}(1^1D_2)$, $\psi_2(1^3D_2)$, and $\psi_3(1^3D_3)$. In our calculations, the instantaneous Bethe–Salpeter method is applied to obtain the hadronic matrix elements. This method includes relativistic corrections which are important especially for the higher orbital excited states. For the semileptonic decay channels with electron as the final lepton, we get the branching ratios $\mathcal{B}[B_c \to \eta_{c2} e\bar{\nu}_e] = 5.9^{-0.8}_{+1.0} \times 10^{-4}$, $\mathcal{B}[B_c \to \psi_2 e\bar{\nu}_e] = 1.5^{-0.2}_{+0.3} \times 10^{-4}$, and $\mathcal{B}[B_c \to \psi_3 e\bar{\nu}_e] = 3.5^{-0.6}_{+0.8} \times 10^{-4}$. The transition form factors, forward–backward asymmetries, and lepton spectra in these processes are also presented. For the nonleptonic decay channels, those with ρ as the lighter meson have the largest branching ratios, $\mathcal{B}[B_c \to \eta_{c2}\rho] = 8.1^{-1.0}_{+1.0} \times 10^{-4}$, $\mathcal{B}[B_c \to \psi_2\rho] = 9.6^{-1.0}_{+1.0} \times 10^{-5}$, and $\mathcal{B}[B_c \to \psi_3\rho] = 4.1^{-0.7}_{+0.8} \times 10^{-4}$.

1 Introduction

In 2013, the Belle Collaboration reported the evidence of a new resonance $X(3823)$ in the B decay channel $B^\pm \to X(\to \chi_{c1}\gamma)K^\pm$ with a statistical significance of 3.8σ [1]. And very recently, the BESIII Collaboration verified its existence with a statistical significance of 6.2σ [2]. Both groups got a similar mass and ratio of the partial decay widths for this particle. On one hand, this state has a mass of $3821.7 \pm 1.3(\text{stat}) \pm 0.7(\text{syst})\ \text{MeV}/c^2$, which is very near the mass value of the 1^3D_2 charmonium predicted by potential models [3,4]; on the other hand, the electromagnetic decay channels $\chi_{c1}\gamma$ and $\chi_{c2}\gamma$ are observed while the later one is suppressed, which means the 1^1D_2 and 1^3D_3 charmonia cases are excluded.

To confirm the above experimental results and compare with other theoretical predictions, studying the properties of D-wave charmonia in a different approach is relevant. In this work we study the $\psi_2(1^3D_2)$ and its two partners $\eta_{c2}(1^1D_2)$ and $\psi_3(1^3D_3)$ in the weak decays of the B_c meson which has attracted lots of attention since its discovery by the CDF Collaboration at Fermilab [5]. Unlike the charmonia and bottomonia, which are hidden-flavor bound states, the B_c meson, which consists of a bottom quark and a charm quark, is open-flavor. Besides that, it is the ground state, which means it cannot decay through strong or electromagnetic interaction. So the B_c meson provides an ideal platform to study the weak interaction.

The semileptonic and nonleptonic transitions of the B_c meson into charmonium states are important processes. Experimentally, only those with J/ψ or $\psi(2S)$ as the final charmonium have been detected [6]. As the LHC accumulates more and more data, the weak decay processes of the B_c meson to charmonia with other quantum numbers will have more possibilities to be detected. That is to say, this is an alternative way to study the charmonia, especially those have not yet been discovered, such as $\eta_{c2}(1^1D_2)$ and $\psi_3(1^3D_3)$. Theoretically, the semileptonic and nonleptonic transitions of the B_c meson into S-wave charmonium states are studied widely by several phenomenological models, such as the relativistic constituent quark model [7–12], the non-relativistic constituent quark model [13], the technique of hard and soft factorization [14] and QCD factorization [15], QCD sum rules [16], Light-cone sum rules [17], the perturbative QCD approach [18–21], and NRQCD [22,23]. There are also some theoretical models to study the processes of B_c decay to a P-wave charmonium [8,24–28], while we lack the information of B_c decay to a D-wave charmonium.

Here we will use the Bethe–Salpeter (BS) method to investigate the exclusive semileptonic and nonleptonic decays of the B_c meson to the D-wave charmonium. This method has been used to study processes with P-wave charmonium [24,28]. As is well known, the BS equation [29] is

[a] e-mail: lrhit@protonmail.com
[b] e-mail: thwang@hit.edu.cn
[c] e-mail: jiangure@hit.edu.cn
[d] e-mail: hanyuan@hit.edu.cn
[e] e-mail: gl_wang@hit.edu.cn

a relativistic two-body bound state equation. To solve BS equation of D-wave mesons and get the corresponding wave function and mass spectra, we use the instantaneous approximation, that is, we solve the Salpeter equations [30] which has been widely used for bound states decay problems [31–34].

This paper is organized as follows. In Sect. 2 we present the general formalism for semileptonic and nonleptonic decay widths of B_c into D-wave charmonia. In Sect. 3 we give the analytic expressions of the corresponding form factors given by the BS method. In Sect. 4, the numerical results are obtained and we compare our results with others', also the theoretical uncertainties and lepton spectra are presented in this section. Section 5 is a short summary of this work. Some bulky analytical expressions are presented in the appendix.

2 Formalisms of semileptonic and nonleptonic decays

In this section we will derive the general formalism for the calculations of both semileptonic and nonleptonic decay widths of B_c meson.

2.1 The semileptonic decay

The semileptonic decays of the B_c meson into D-wave charmonia are three-body decay processes. We consider the neutrinos as massless fermions. The differential form of the three-body decay width can be written as

$$\mathrm{d}\Gamma = \frac{1}{(2\pi)^3}\frac{1}{32M^3}\overline{|\mathcal{M}|^2}\mathrm{d}m_{12}^2\mathrm{d}m_{23}^2, \tag{1}$$

where M is the mass of B_c; m_{12} is the invariant mass of final $c\bar{c}$ meson and neutrino which is defined as $m_{12}^2 = (P_F+p_\nu)^2$; m_{23} is the invariant mass of final neutrino and charged lepton, which is defined as $m_{23}^2 = (p_\nu + p_\ell)^2$. Here we have used P_F, p_ν, and p_ℓ to denote the 4-momentum of final $c\bar{c}$ meson, neutrino, and charged lepton, respectively. $\mathcal{M}$ is the invariant amplitude of this process. In the above equation we have summed over the polarizations of final states.

2.1.1 Form factors

The Feynman diagram involved in the semileptonic decays of B_c meson in the tree level is showed in Fig. 1. The invariant amplitude $\mathcal{M}$ can be written directly as

$$\mathcal{M} = \frac{G_F}{\sqrt{2}}V_{cb}\langle c\bar{c}|h^\mu|B_c\rangle\bar{u}_\ell(p_\ell)\Gamma_\mu v_\nu(p_\nu), \tag{2}$$

where G_F is the Fermi constant; V_{cb} is the CKM matrix element for the $b\to c$ transition; $\langle c\bar{c}|h^\mu|B_c\rangle$ is the hadronic matrix element; $h^\mu = \bar{c}\Gamma^\mu b$ is the weak charged current and $\Gamma^\mu = \gamma^\mu(1-\gamma^5)$. The general form of the hadronic matrix

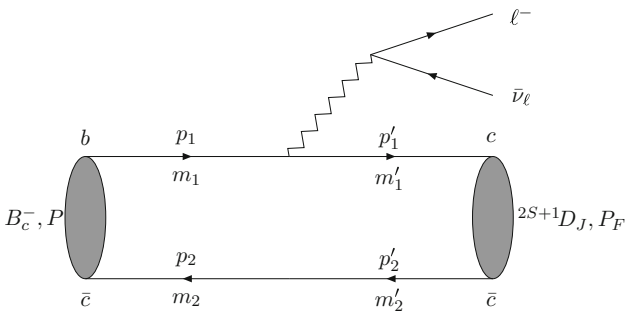

Fig. 1 Feynman diagram of the semileptonic decay of B_c into D-wave charmonia. P and P_F are the momenta of initial and final mesons, respectively. S, D, and J are quantum numbers of spin, orbital angular momentum and total angular momentum for the final $c\bar{c}$ system, respectively

element $\langle c\bar{c}|h^\mu|B_c\rangle$ depends on the total angular momentum J of the final meson. For η_{c2}, $J=2$, the transition matrix can be written as

$$\langle c\bar{c}|h^\mu|B_c\rangle = e_{\alpha\beta}P^\alpha(s_1P^\beta P^\mu + s_2P^\beta P_F^\mu + s_3g^{\beta\mu} + \mathrm{i}s_4\epsilon^{\mu\beta PP_F}), \tag{3}$$

where $g^{\beta\mu}$ is the Minkowski metric tensor. We have used the definition $\epsilon_{\mu\nu PP_F} \equiv \epsilon_{\mu\nu\alpha\beta}P^\alpha P_F^\beta$; $\epsilon_{\mu\nu\alpha\beta}$ is the totally antisymmetric tensor; $e_{\alpha\beta}$ is the polarization tensor of the charmonium with $J=2$; s_1, s_2, s_3, and s_4 are the form factors for the $^1D_2$ state; for $^3D_2$ state the relation between $\langle c\bar{c}|h^\mu|B_c\rangle$ and form factors t_i ($i=1,2,3,4$) has the same form with $^1D_2$ just s_i replaced with t_i. For the $J=3$ meson, the hadronic matrix element can be described by the form factors h_i:

$$\langle c\bar{c}|h^\mu|B_c\rangle = e_{\alpha\beta\gamma}P^\alpha P^\beta(h_1P^\gamma P^\mu + h_2P^\gamma P_F^\mu + h_3g^{\gamma\mu} + \mathrm{i}h_4\epsilon^{\mu\gamma PP_F}), \tag{4}$$

where $e_{\alpha\beta\gamma}$ is the polarization tensor for the meson with $J=3$. The expressions of these form factors are given in the next section.

The squared transition matrix element with the summed polarizations of final states (see Eq. (1)) has the form

$$\overline{|\mathcal{M}|^2} = \frac{G_F^2}{2}|V_{cb}|^2L^{\mu\nu}H_{\mu\nu}. \tag{5}$$

In the above equation $L^{\mu\nu}$ is the leptonic tensor

$$\begin{aligned}L^{\mu\nu} &= \sum_{s_\ell,s_\nu}[\bar{u}_\ell(p_\ell)\Gamma^\mu v_\nu(p_\nu)][\bar{u}_\ell(p_\ell)\Gamma^\nu v_\nu(p_\nu)]^\dagger \\ &= 8(p_\ell^\mu p_\nu^\nu + p_\nu^\mu p_\ell^\nu - p_\ell\cdot p_\nu g^{\mu\nu} - \mathrm{i}\epsilon^{\mu\nu p_\ell p_\nu}),\end{aligned} \tag{6}$$

and $H_{\mu\nu}$ is the hadronic tensor, which can be written as

$$H_{\mu\nu} = N_1P_\mu P_\nu + N_2(P_\mu P_{F\nu} + P_\nu P_{F\mu}) + N_4P_{F\mu}P_{F\nu} + N_5g_{\mu\nu} + \mathrm{i}N_6\epsilon_{\mu\nu PP_F}, \tag{7}$$

where N_i $(i = 1, 2, 4, 5, 6)$ is described by form factors s_j, t_j or h_j $(j = 1, 2, 3, 4)$ (see Appendix A). By using Eqs. (6) and (7), we can write $L^{\mu\nu}H_{\mu\nu}$ as follows:

$$\begin{aligned} L^{\mu\nu}H_{\mu\nu} = {} & 8N_1(2P\cdot p_\ell P\cdot p_\nu - M^2 p_\nu\cdot p_\ell) \\ & + 16N_2(P\cdot p_\ell P_F\cdot p_\nu \\ & + P_F\cdot p_\ell P\cdot p_\nu - p_\nu\cdot p_\ell P\cdot P_F) \\ & + 8N_4(2P_F\cdot p_\ell P_F\cdot p_\nu - M_F^2 p_\nu\cdot p_\ell) \\ & - 16N_5 p_\nu\cdot p_\ell + 16N_6(P_F\cdot p_\ell P\cdot p_\nu \\ & - P\cdot p_\ell P_F\cdot p_\nu), \end{aligned} \tag{8}$$

where M_F stands for the mass of final charmonium meson.

2.1.2 Angular distribution and lepton spectra

The angular distribution of semileptonic decays of B_c to D-wave charmonia can be described as

$$\frac{\mathrm{d}\Gamma}{\mathrm{d}\cos\theta} = \int \frac{1}{(2\pi)^3}\frac{|\boldsymbol{p}_\ell^*||\boldsymbol{p}_F^*|}{16M^3}\overline{|\mathcal{M}|^2}\mathrm{d}m_{23}^2, \tag{9}$$

where $\boldsymbol{p}_\ell^*$ and $\boldsymbol{p}_F^*$ are respectively the 3-momenta of the charged lepton and the final charmonium in the rest frame of lepton–neutrino system, which have the form $|\boldsymbol{p}_\ell^*| = \lambda^{\frac{1}{2}}(m_{23}^2, M_\ell^2, M_\nu^2)/(2m_{23})$ and $|\boldsymbol{p}_F^*| = \lambda^{\frac{1}{2}}(m_{23}^2, M^2, M_F^2)/(2m_{23})$. Here we used the Källen function $\lambda(a, b, c) = (a^2 + b^2 + c^2 - 2ab - 2bc - 2ac)$. M_ℓ and M_ν are the masses of the charged lepton and neutrino, respectively. θ is angle between $\boldsymbol{p}_\ell^*$ and $\boldsymbol{p}_F^*$. The forward–backward asymmetry A_{FB} is another quantity we are interested in; it is defined as

$$A_{FB} = \frac{\Gamma_{\cos\theta>0} - \Gamma_{\cos\theta<0}}{\Gamma_{\cos\theta>0} + \Gamma_{\cos\theta<0}}. \tag{10}$$

One can check that A_{FB} has the same value for the decays of B_c^+ and B_c^- mesons. Its numerical results are given in Sect. 4. The momentum spectrum of the charged lepton in the semileptonic decays is also an important quantity both experimentally and theoretically. It has the form

$$\frac{\mathrm{d}\Gamma}{\mathrm{d}|\boldsymbol{p}_\ell|} = \int \frac{1}{(2\pi)^3}\frac{|\boldsymbol{p}_\ell|}{16M^2E_\ell}\overline{|\mathcal{M}|^2}\mathrm{d}m_{23}^2, \tag{11}$$

where E_ℓ is the energy of the charged lepton in the B_c rest frame.

2.2 Nonleptonic decay formalism

In this section, we will deal with the nonleptonic decays in the framework of the factorization approximation [35,36]. The Feynman diagram of the nonleptonic decay of the B_c meson is showed in Fig. 2. In this work we only calculate the processes when X is π, ρ, K, or K^*.

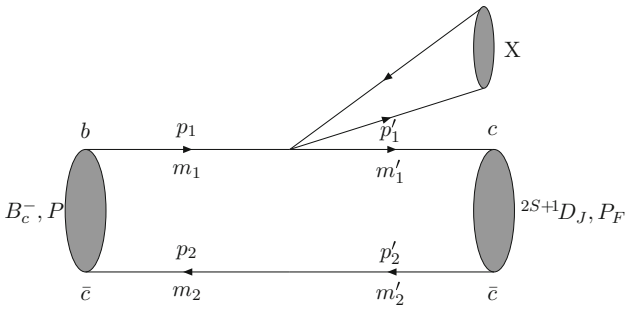

Fig. 2 The Feynman diagram of the nonleptonic decay of B_c meson to D-wave charmonia. X denotes a light meson

The effective Hamiltonian for this process is [37]

$$H_{\mathrm{eff}} = \frac{G_F}{\sqrt{2}}V_{cb}[c_1(\mu)O_1 + c_2(\mu)O_2] + \mathrm{h.c.}, \tag{12}$$

where $c_1(\mu)$ and $c_2(\mu)$ are the scale-dependent Wilson coefficients. O_is are the relevant four-quark local operators, which have the following forms:

$$O_1 = [V_{ud}(\bar{d}_\alpha u_\alpha)_{V-A} + V_{us}(\bar{s}_\alpha u_\alpha)_{V-A}](\bar{c}_\beta b_\beta)_{V-A}, \tag{13}$$
$$O_2 = [V_{ud}(\bar{d}_\alpha u_\beta)_{V-A} + V_{us}(\bar{s}_\alpha u_\beta)_{V-A}](\bar{c}_\beta b_\alpha)_{V-A}, \tag{14}$$

where we have used the symbol $(\bar{q}_1 q_2)_{V-A} = \bar{q}_1\gamma^\mu(1 - \gamma^5)q_2$; here α and β denote the color indices.

As a primary study, in this work the nonleptonic B_c decays are calculated with the factorization approximation, which has been widely used in heavy mesons' weak decays [7,9,13,38]. In this approximation, the decay amplitude is factorized as the product of two parts, namely, the hadronic transition matrix element and an annihilation matrix element. The factorization assumption is expected to hold for processes that involve a heavy meson and a light meson, provided the light meson is energetic [39]. Then we can write the nonleptonic decay amplitude as

$$\begin{aligned} & \mathcal{M}\big[B_c \to (c\bar{c})X\big] \\ & \simeq \frac{G_F}{\sqrt{2}}V_{bc}V_{q_1q_2}a_1(\mu)\langle c\bar{c}|h_{bc}^\mu|B_c\rangle\langle X|J_\mu|0\rangle. \end{aligned} \tag{15}$$

In the above equation we have used the definitions $J_\mu = (\bar{q}_1 q_2)_{V-A}$; $a_1 = c_1 + \frac{1}{N_c}c_2$, where $N_c = 3$ is the number of colors. We take $\mu = m_b$ for the b decays and $a_1 = 1.14, a_2 = -0.2$ [9] are used in this work. To estimate the systematic uncertainties from non-factorizable contributions, we treat the N_c as an adjustable parameter varying from 2 to $+\infty$ [40], and then we calculate the deviation to the central values. We stress that the factorization method used here is just taken as a preliminary study for the nonleptonic decays.

The annihilation matrix element can be expressed by the decay constant and the momentum (P_X) or the polarization vector (e^μ) of X meson

$$\langle X|J^{\mu}|0\rangle = \begin{cases} \mathrm{i} f_P P_X^{\mu} & \text{X is a pseudoscalar meson,} \quad (16a) \\ f_V M_X e^{\mu} & \text{X is a vector meson.} \quad (16b) \end{cases}$$

M_X is the mass of the X meson, f_P and f_V are the corresponding decay constants.

Finally, we get the nonleptonic decay width of the B_c meson

$$\Gamma = \frac{|\boldsymbol{p}|}{8\pi M^2}\overline{|\mathcal{M}|^2}, \tag{17}$$

where $\boldsymbol{p}$ represents the 3-momentum of either of the two final mesons in the B_c rest frame, which is expressed as $|\boldsymbol{p}| = \lambda^{\frac{1}{2}}(M^2, M_X^2, M_F^2)/(2M)$.

3 Hadronic matrix element

In this section we will calculate the hadronic matrix element using the BS method. First we briefly review the instantaneous Bethe–Salpeter methods. Then we calculate the hadronic matrix transition element with the corresponding BS wave function. Finally the form factors are given graphically.

3.1 Introduction to BS methods

It is well known that the BS equation in momentum space reads [29]

$$(\not{p}_1 - m_1)\Psi(q)(\not{p}_2 + m_2) = \mathrm{i}\int \frac{\mathrm{d}^4k}{(2\pi)^4} V(q-k)\Psi(k), \tag{18}$$

where $\Psi(q)$ stands for the BS wave function; $V(q-k)$ is the BS interaction kernel; p_1 and p_2 are the momenta of constituent quark and anti-quark in the meson; m_1 and m_2 are the corresponding masses of constituent quark and anti-quark respectively (see Fig. 1). p_1 and p_2 can be described with the meson total momentum P and inner relative momentum q as

$$\begin{cases} p_1 = \alpha_1 P + q, & \alpha_1 = \frac{m_1}{m_1+m_2}, \\ p_2 = \alpha_2 P - q, & \alpha_2 = \frac{m_2}{m_1+m_2}. \end{cases} \tag{19}$$

In the instantaneous approximation [30], $V(q-k) \sim V(|\boldsymbol{q}-\boldsymbol{k}|)$ does not depend on the time component of $(q-k)$. By using the same method in Ref. [30], we introduce the 3-dimensional Salpeter wave function $\varphi(q_\perp)$ and integration $\eta(q_\perp)$ as

$$\varphi(q_\perp) = \mathrm{i}\int \frac{\mathrm{d}q_P}{2\pi}\Psi(q), \tag{20}$$

$$\eta(q_\perp) = \int \frac{\mathrm{d}^3k_\perp}{(2\pi)^3} V(|q_\perp - k_\perp|)\varphi(k_\perp), \tag{21}$$

where $q_P = \frac{P\cdot q}{M}$ and $q_\perp = q - \frac{P}{M}q_P$, in rest frame of initial meson they correspond to the q^0 and $\boldsymbol{q}$ respectively; the integration $\eta(q_\perp)$ can be understood as the BS vertex for bound state. Now the BS equation (18) can be written as

$$\Psi(q) = S(p_1)\eta(q_\perp)S(-p_2). \tag{22}$$

$S(p_1)$ and $S(-p_2)$ are the propagators for the quark and anti-quark, respectively, and can be decomposed as

$$\begin{aligned} S(+p_1) &= \frac{\mathrm{i}\Lambda_1^+}{q_P + \alpha_1 M - \omega_1 + \mathrm{i}\epsilon} + \frac{\mathrm{i}\Lambda_1^-}{q_P + \alpha_1 M + \omega_1 - \mathrm{i}\epsilon}, \\ S(-p_2) &= \frac{\mathrm{i}\Lambda_2^+}{q_P - \alpha_2 M + \omega_2 - \mathrm{i}\epsilon} + \frac{\mathrm{i}\Lambda_2^-}{q_P + \alpha_2 M - \omega_2 + \mathrm{i}\epsilon}, \end{aligned} \tag{23}$$

where $\omega_i = \sqrt{m_i^2 - q_\perp^2}$ $(i = 1, 2)$ and projection operators $\Lambda_i^{\pm}(q_\perp)$ $(i = 1$ for quark and 2 for anti-quark) are defined as

$$\Lambda_i^{\pm} = \frac{1}{2\omega_i}\left[\frac{\not{P}}{M}\omega_i \pm (-1)^{i+1}(m_i + \not{q}_\perp)\right]. \tag{24}$$

Since the BS kernel is instantaneous, we can perform contour integration over q_P on both sides of Eq. (22) and then we obtain the coupled Salpeter equations [30]

$$\begin{cases} (M - \omega_1 - \omega_2)\varphi^{++} = +\Lambda_1^+(q_\perp)\eta(q_\perp)\Lambda_2^+(q_\perp), & (25a) \\ (M + \omega_1 + \omega_2)\varphi^{--} = -\Lambda_1^-(q_\perp)\eta(q_\perp)\Lambda_2^-(q_\perp), & (25b) \\ \varphi^{+-} = \varphi^{-+} = 0, & (25c) \end{cases}$$

where $\varphi^{\pm\pm}$ are related to φ by

$$\varphi^{\pm\pm} \equiv \Lambda_1^{\pm}(q_\perp)\frac{\not{P}}{M}\varphi(q_\perp)\frac{\not{P}}{M}\Lambda_2^{\pm}(q_\perp), \tag{26}$$

$$\varphi = \varphi^{++} + \varphi^{-+} + \varphi^{+-} + \varphi^{--}. \tag{27}$$

The normalization condition for BS equation now reads

$$\int \frac{\mathrm{d}^3k_\perp}{(2\pi)^3}\left[\overline{\varphi}^{++}\frac{\not{P}}{M}\varphi^{++}\frac{\not{P}}{M} - \overline{\varphi}^{--}\frac{\not{P}}{M}\varphi^{--}\frac{\not{P}}{M}\right] = 2M. \tag{28}$$

3.2 Numerical results of Salpeter equations

To solve the Salpeter equations numerically, first we choose the Cornell potential as the interaction kernel, which has the following forms [41]:

$$
\begin{aligned}
V(\boldsymbol{q}) &= (2\pi)^3 V_s(\boldsymbol{q}) + \gamma^0 \otimes \gamma_0 (2\pi)^3 V_v(\boldsymbol{q}),\\
V_s(\boldsymbol{q}) &= -\left(\frac{\lambda}{\alpha} + V_0\right)\delta^3(\boldsymbol{q}) + \frac{\lambda}{\pi^2(\boldsymbol{q}^2+\alpha^2)^2},\\
V_v(\boldsymbol{q}) &= -\frac{2\alpha_s(\boldsymbol{q})}{3\pi^2(\boldsymbol{q}^2+\alpha^2)},\\
\alpha_s(\boldsymbol{q}) &= \frac{12\pi}{27\ln(a+\frac{\boldsymbol{q}^2}{\Lambda_{\rm QCD}})}.
\end{aligned}
\tag{29}
$$

In the above equations the symbol $\otimes$ denotes that the BS wave functions are sandwiched between the two γ^0 matrix. The model parameters we used are the same as before [42], reading

$$
\begin{aligned}
&a = e = 2.7183, \quad \alpha = 0.06\ \text{GeV}, \quad \lambda = 0.21\ \text{GeV},\\
&m_c = 1.62\ \text{GeV}, \quad m_b = 4.96\ \text{GeV}, \quad \Lambda_{\rm QCD} = 0.27\ \text{GeV}.
\end{aligned}
$$

Now we just take the $0^-(^1S_0)$ state as an example to show how to solve the full coupled Salpeter equations to obtain the numerical results. The Salpeter wave function for the $0^-(^1S_0)$ state has the following general form [41]:

$$
\varphi(^1S_0) = M\left[k_1\frac{\not{P}}{M} + k_2 + k_3\frac{\not{q}_\perp}{M} + k_4\frac{\not{P}\not{q}_\perp}{M^2}\right]\gamma^5. \tag{30}
$$

By utilizing the Salpeter equation (25c), we can obtain the following two constraint conditions:

$$
\begin{aligned}
k_3 &= +\frac{M(\omega_1-\omega_2)}{m_1\omega_2+m_2\omega_1}k_2,\\
k_4 &= -\frac{M(\omega_1+\omega_2)}{m_1\omega_2+m_2\omega_1}k_1.
\end{aligned}
\tag{31}
$$

Now in the above $^1S_0$ state Salpeter wave function, there are only two undetermined wave functions k_1 and k_2, which are just the functions of $q_\perp^2$.

By using the definition Eq. (26), the positive wave function for the $^1S_0$ state can be written as

$$
\varphi^{++}(^1S_0) = \left[A_1 + A_2\frac{\not{P}}{M} + A_3\frac{\not{q}_\perp}{M} + A_4\frac{\not{P}\not{q}_\perp}{M^2}\right]\gamma^5. \tag{32}
$$

A_i $(i = 1, 2, 3, 4)$ have the following forms:

$$
\begin{aligned}
A_1 &= \frac{M}{2}\left[\frac{\omega_1+\omega_2}{m_1+m_2}k_1 + k_2\right],\\
A_2 &= \frac{M}{2}\left[k_1 + \frac{m_1+m_2}{\omega_1+\omega_2}k_2\right],\\
A_3 &= -\frac{M(\omega_1-\omega_2)}{m_1\omega_2+m_2\omega_1}A_1,\\
A_4 &= -\frac{M(m_1+m_2)}{m_1\omega_2+m_2\omega_1}A_1.
\end{aligned}
\tag{33}
$$

Similarly, the $\varphi^{--}(^1S_0)$ is expressed as

$$
\varphi^{--}(^1S_0) = \left[Z_1 + Z_2\frac{\not{P}}{M} + Z_3\frac{\not{q}_\perp}{M} + Z_4\frac{\not{P}\not{q}_\perp}{M^2}\right]\gamma^5. \tag{34}
$$

Z_i $(i = 1, 2, 3, 4)$ has the following forms:

$$
\begin{aligned}
Z_1 &= \frac{M}{2}\left[k_2 - \frac{\omega_1+\omega_2}{m_1+m_2}k_1\right],\\
Z_2 &= \frac{M}{2}\left[k_1 - \frac{m_1+m_2}{\omega_1+\omega_2}k_2\right],\\
Z_3 &= -\frac{M(\omega_1-\omega_2)}{m_1\omega_2+m_2\omega_1}Z_1,\\
Z_4 &= +\frac{M(m_1+m_2)}{m_1\omega_2+m_2\omega_1}Z_1.
\end{aligned}
\tag{35}
$$

And now the normalization condition reads

$$
\int\frac{\mathrm{d}^3\boldsymbol{q}}{(2\pi)^3}\frac{8M\omega_1\omega_2k_1k_2}{(m_1\omega_2+m_2\omega_1)} = 1. \tag{36}
$$

Inserting the expressions of $\varphi^{++}(^1S_0)$ and $\varphi^{--}(^1S_0)$ into Eqs. (25a) and (25b), respectively, we can obtain the two coupled eigen equations on k_1 and k_2 [41] as

$$
\begin{cases}
(M-\omega_1-\omega_2)\left[ck_1(\boldsymbol{q}) + k_2(\boldsymbol{q})\right]\\
\quad = \frac{1}{2\omega_1\omega_2}\int\mathrm{d}^3\boldsymbol{k}\left[H_1k_1(\boldsymbol{k}) + H_2k_2(\boldsymbol{k})\right],\\
(M+\omega_1+\omega_2)\left[k_2(\boldsymbol{q}) - ck_1(\boldsymbol{q})\right]\\
\quad = \frac{1}{2\omega_1\omega_2}\int\mathrm{d}^3\boldsymbol{k}\left[H_1k_1(\boldsymbol{k}) - H_2k_2(\boldsymbol{k})\right],
\end{cases}
\tag{37}
$$

where we have used definition $c = \frac{\omega_1+\omega_2}{m_1+m_2}$ and the shorthand

$$
\begin{aligned}
H_1 &= \boldsymbol{k}\cdot\boldsymbol{q}(V_s+V_v)\frac{(v_1+v_2)(\omega_1+\omega_2)}{m_1v_2+m_2v_1}\\
&\quad -(V_s-V_v)(m_1\omega_2+m_2\omega_1),\\
H_2 &= \boldsymbol{k}\cdot\boldsymbol{q}(V_s+V_v)\frac{(v_1-v_2)(m_1-m_2)}{m_1v_2+m_2v_1}\\
&\quad -(V_s-V_v)(m_1m_2+\omega_1\omega_2+\boldsymbol{q}^2).
\end{aligned}
\tag{38}
$$

In the above equations we have defined $v_i = \sqrt{m_i^2+\boldsymbol{k}^2}$ $(i = 1, 2)$. Then by solving the two coupled eigen equations, we obtain the mass spectrum and corresponding wave functions k_1 and k_2. Repeating the similar procedures we can obtain the numerical wave functions for $2^{-+}(^1D_2)$, $2^{--}(^3D_2)$, and $3^{--}(^3D_3)$. The interested reader can find more details of solving the full Salpeter equations in Refs. [34,41,42].

3.3 Form factors for hadronic transition

Now we will calculate the form factors with BS methods. According to Mandelstam formalism [43], the hadronic tran-

sition matrix element $\langle c\bar{c}|h^{\mu}|B_c\rangle$ can be directly written as

$$\begin{aligned}\langle c\bar{c}|h^{\mu}|B_c\rangle &= \mathrm{i}\int\frac{\mathrm{d}^4q\mathrm{d}^4q'}{(2\pi)^4}\mathrm{Tr}[\bar{\Psi}(q')\Gamma^{\mu}\Psi(q)S^{-1}\\ &\quad\times(-p_2)\delta^{(4)}(p_2-p_2')]\\ &= \mathrm{i}\int\frac{\mathrm{d}^4q}{(2\pi)^4}\mathrm{Tr}[\bar{\Psi}(q')\Gamma^{\mu}\Psi(q)S^{-1}(-p_2)]. \quad (39)\end{aligned}$$

In the above expression, $\Psi(q')$ stands for the BS wave function of final $c\bar{c}$ systems and $\bar{\Psi}=\gamma^0\Psi^{\dagger}\gamma^0$; q' is the inner relative momentum of the $c\bar{c}$ system, which is related to the quark (anti-quark) momentum p_1' (p_2') by $p_i'=\alpha_i'P_F+(-1)^{i+1}q'$ and $\alpha_i'=\frac{m_i'}{m_1'+m_2'}$ ($i=1,2$), where m_i' are masses of the constituent quarks in the final bound states (see Fig. 1); here we have $m_1=m_b$, $m_2=m_2'=m_1'=m_c$; $S^{-1}(-p_2)=(-\not{p}_2-m_2)$ is the inverse of propagator for anti-quark. Since the propagator S_2 is used by both initial and final mesons, here we add an $S^{-1}(-p_2)$ factor. As there is a delta function in the first line of the above equation, the relative momenta q and q' are related by $q'=q-(\alpha_2P-\alpha_2'P_F)$.

By inserting Eqs. (22) and (23) into Eq. (39), then performing the counter integral over q_P, we get

$$\begin{aligned}\langle c\bar{c}|h^{\mu}|B_c\rangle = \int\frac{\mathrm{d}^3q_{\perp}}{(2\pi)^3}\mathrm{Tr}\Big\{&\frac{\not{P}}{M}(\bar{\varphi}'^{++}\Gamma^{\mu}\varphi^{++}+\bar{\varphi}'^{++}\Gamma^{\mu}\psi^{-+}\\ &-\bar{\psi}'^{-+}\Gamma^{\mu}\varphi^{--}+\bar{\psi}'^{+-}\Gamma^{\mu}\varphi^{++} \quad (40)\\ &-\bar{\varphi}'^{--}\Gamma^{\mu}\psi^{+-}-\bar{\varphi}'^{--}\Gamma^{\mu}\varphi^{--})\Big\}, \quad (41)\end{aligned}$$

where we have used the following definitions:

$$\begin{aligned}\psi^{-+} &= \frac{\Lambda_1^-\eta\Lambda_2^+}{(\omega_1'+\omega_1)+(M-E')},\\ \bar{\psi}'^{-+} &= \frac{\Lambda_2'^-\bar{\eta}'\Lambda_1'^+}{(\omega_1'+\omega_1)+(M-E')},\\ \psi^{+-} &= \frac{\Lambda_1^+\eta\Lambda_2^-}{(\omega_1'+\omega_1)-(M-E')},\\ \bar{\psi}'^{+-} &= \frac{\Lambda_2'^+\bar{\eta}'\Lambda_1'^-}{(\omega_1'+\omega_1)-(M-E')}.\end{aligned} \quad (42)$$

φ^{++} is the Salpeter positive wave function, which is much larger than ψ^{-+}, ψ^{+-} and φ^{--} in the case of weak binding [7,44]. In the following calculations we will only consider the dominant $[\bar{\varphi}'^{++}\Gamma^{\mu}\varphi^{++}]$ part, while other contributions are ignored. The reliability of this approximation can be seen in Ref. [28]. Finally we obtain the form factors described with the 3-dimensional Salpeter positive wave function

$$\langle c\bar{c}|h^{\mu}_{bc}|B_c\rangle = \int\frac{\mathrm{d}^3q_{\perp}}{(2\pi)^3}\mathrm{Tr}\Big[\frac{\not{P}}{M}\bar{\varphi}'^{++}(q_{\perp}')\Gamma^{\mu}\varphi^{++}(q_{\perp})\Big]. \quad (43)$$

In our calculation, the final charmonium states are $^1D_2(2^{-+})$, $^3D_2(2^{--})$, or $^3D_3(3^{--})$. Their BS wave functions are constructed by considering the spin and parity of the corresponding mesons [45]. We will take the $^1D_2(2^{-+})$ state as an example to show how to do the calculation to obtain the form factors. The results of other mesons will be given directly.

The Salpeter wave function of the $^1D_2$ states with equal mass can be written as [42]

$$\varphi_{2^{-+}} = e^{\mu\nu}q'_{\mu\perp}q'_{\nu\perp}\Big[f_1+f_2\frac{\not{P}_F}{M_F}+f_4\frac{\not{P}_F\not{q}'_{\perp}}{M_F^2}\Big]. \quad (44)$$

And Salpeter equation (25c) gives the constraint condition $f_4=-\frac{M_F}{m_c}f_2$, where m_c is the c quark constituent mass; $e^{\mu\nu}$ is the symmetric polarization tensor for $J=2$, which satisfies the following relations [46]:

$$e^{\mu\nu}P_{F\mu}=0, \quad e^{\mu\nu}g_{\mu\nu}=0. \quad (45)$$

And the completeness relation for the polarization tensor is

$$\sum_{m=-2}^{2}e^{\mu\nu}(m)e^{\alpha\beta}(m)=\frac{1}{2}\big(g_{\perp}^{\alpha\mu}g_{\perp}^{\beta\nu}+g_{\perp}^{\alpha\nu}g_{\perp}^{\beta\mu}\big)-\frac{1}{3}g_{\perp}^{\alpha\beta}g_{\perp}^{\mu\nu}, \quad (46)$$

where we have defined $g_{\perp}^{\alpha\beta}\equiv-g^{\alpha\beta}+\frac{P_F^{\alpha}P_F^{\beta}}{P_F^2}$.

From the definition, we get the Salpeter positive wave function for $^1D_2(2^{-+})$ charmonium [42] as

$$\varphi^{++}(^1D_2)=e^{\mu\nu}q'_{\mu\perp}q'_{\nu\perp}\Big[B_1+B_2\frac{\not{P}_F}{M_F}+B_4\frac{\not{P}_F\not{q}'_{\perp}}{M_F^2}\Big]\gamma^5; \quad (47)$$

$$\begin{aligned}B_1 &= \frac{1}{2}\Big[f_1+\frac{\omega_c}{m_c}f_2\Big],\\ B_2 &= \frac{1}{2}\Big[f_2+\frac{m_c}{\omega_c}f_1\Big],\\ B_4 &= -\frac{M_F}{\omega_c}B_1,\end{aligned} \quad (48)$$

where $\omega_c=\sqrt{m_c^2-q_{\perp}'^2}$; f_1 and f_2 are functions of $q'_{\perp}$.

Having theses wave functions, we can deal with the form factors in the hadronic matrix element. For the transition $B_c\to\eta_{c2}$, inserting Eqs. (32) and (47) into Eq. (43) and finishing the trace, we obtain the form factors s_1, s_2, s_3, and s_4 in Eq. (3)

$$
\begin{aligned}
s_1 &= \int \frac{\mathrm{d}^3\boldsymbol{q}}{(2\pi)^3}\Bigg[x_1 - \frac{C_1 E_F(x_3+x_4)}{Mp_F} \\
&\quad + \frac{(x_6+x_7)(C_{21}E_F^2 - C_{22}p_F^2)}{M^2 p_F^2} \\
&\quad + \frac{E_F x_9(3C_{32}p_F^2 - C_{31}E_F^2)}{M^3 p_F^3}\Bigg], \\
s_2 &= \int \frac{\mathrm{d}^3\boldsymbol{q}}{(2\pi)^3}\Bigg[x_2 + \frac{C_1(Mx_3 - E_F x_5)}{Mp_F} \\
&\quad + \frac{C_{21}E_F(E_F x_8 - Mx_6)}{M^2 p_F^2} - \frac{C_{22}x_8}{M^2} \\
&\quad + \frac{x_9(C_{31}E_F^2 - C_{32}p_F^2)}{M^2 p_F^3}\Bigg], \\
s_3 &= \int \frac{\mathrm{d}^3\boldsymbol{q}}{(2\pi)^3}\left(C_{22}x_6 - \frac{2C_{32}E_F x_9}{Mp_F}\right), \\
s_4 &= \int \frac{\mathrm{d}^3\boldsymbol{q}}{(2\pi)^3}\left(C_{22}x_{10} - \frac{2C_{32}E_F x_{11}}{Mp_F}\right).
\end{aligned}
\tag{49}
$$

In the above expressions, p_F denotes the absolute value of $\boldsymbol{P}_F$, which is the 3-momentum of the final charmonium, $E_F = \sqrt{M_F^2 + p_F^2}$. The specific expressions of x_i ($i = 1, 2, \ldots, 11$) can be found in Appendix B. C_i are expressed as

$$
\begin{cases}
C_1 = |\boldsymbol{q}|\cos\eta, & C_{21} = \frac{1}{2}|\boldsymbol{q}|^2(3\cos^2\eta - 1), \\
C_{22} = \frac{1}{2}|\boldsymbol{q}|^2(\cos^2\eta - 1), & C_{31} = \frac{1}{2}|\boldsymbol{q}|^3(5\cos^3\eta - 3\cos\eta), \\
C_{32} = \frac{1}{2}|\boldsymbol{q}|^3(\cos^3\eta - \cos\eta), & C_{41} = \frac{1}{8}|\boldsymbol{q}|^4(35\cos^4\eta - 30\cos^2\eta + 3), \\
C_{42} = \frac{1}{8}|\boldsymbol{q}|^4(5\cos^4\eta - 6\cos^2\eta + 1), & C_{43} = \frac{1}{8}|\boldsymbol{q}|^4(\cos^4\eta - 2\cos^2\eta + 1),
\end{cases}
\tag{50}
$$

where η is the angle between $\boldsymbol{q}$ and $\boldsymbol{P}_F$.

Replacing the wave function $\varphi^{++}(^1D_2)$ by $\varphi^{++}(^3D_2)$ or $\varphi^{++}(^3D_3)$, and repeating the procedures above, we can get the form factors for the transition of B_c to $\psi_2(1^3D_2)$ or $\psi_3(1^3D_3)$ charmonium. The Salpeter positive wave function for $2^{--}(^3D_2)$ and $3^{--}(^3D_3)$ [34] can be found in Appendix C. We will not give the bulky analytical expressions but only present the form factors for the decays to $^3D_2$ and $^3D_3$ charmonia graphically (see Fig. 3).

Finally we can obtain the numerical results of form factors. In Fig. 3a–c, we show the form factors s_i, t_i, and h_i ($i = 1, 2, 3, 4$), which change with momentum transfer t^2, where $t^2 = (P - P_F)^2$. To make the form factors have the same dimension, we have divided s_3, t_3, and h_3 by $M_{B_c}^2$. One can notice that the form factors we got are quite smooth in all the concerned range of t^2. This is important for the calculation of nonleptonic decays, which depends sensitively on one specific point of the form factors.

4 Decay width and discussions

For the $\psi_2(1^3D_2)$ meson, which has been found experimentally to be $X(3823)$ [1]. For $\eta_{c2}(1^1D_2)$ and $\psi_3(1^3D_3)$, we use the predictions of Ref. [49]. The meson masses we used in this work are

$$
M_{B_c} = 6.276\ \text{GeV}, \quad M_{\eta_{c2}} = 3.837\ \text{GeV},
$$
$$
M_{\psi_2} = 3.823\ \text{GeV}, \quad M_{\psi_3} = 3.849\ \text{GeV}.
$$

The lifetime for the B_c meson is $\tau_{B_c} = 0.452 \times 10^{-12}$ s [6]. The values of CKM matrix elements we use in this work are

$$
V_{cb} = 0.041, \quad V_{ud} = 0.974, \quad V_{us} = 0.225.
$$

Among the three D-wave charmonia we calculated here, $\psi_2(1^3D_2)$ and $\eta_{c2}(1^1D_2)$ are expected to be quite narrow since there are no open charm decay modes. Both of them are just above the threshold of $D\bar{D}$ while below $D\bar{D}^*$. However, the conservation of parity forbids the $D\bar{D}$ channel. So the dominant decay modes are expected to be electromagnetic ones. For $\psi_2(1^3D_2)$, the total width are estimated to be ∼0.4 MeV [47]. The predominant EM decay channel of this particle is $\eta_{c2}(1^1D_2) \to h_c(1P)\gamma$ and the corresponding decay width is about 0.3 MeV [4,48]. For $\psi_3(1^3D_3)$, although its mass is above the $D\bar{D}$ threshold, the decay width is estimated to be less than 1 MeV [49,50]. The reasons are that the phase space is small and there is a F-wave centrifugal barrier. The radiative width for the main EM transition $\psi_3(1^3D_3) \to \gamma\chi_{c2}$ is ∼0.3 MeV.

4.1 Branching ratios and lepton spectra for B_c semileptonic decays

From the results of form factors, we can get the branching ratios of B_c exclusive decays. The semileptonic decay widths of B_c to D-wave charmonia are listed in Table 1. For the theoretical uncertainties, here we will just discuss the dependence of the final results on our model parameters λ, Λ_{QCD}, m_b, and m_c in the Cornell potential. The theoretical errors, induced by these four parameters, are determined by varying every parameter by ±5 %, and then scanning the four-parameter space to find the maximum deviation. Generally, this theoretical uncertainties can amount to 10−20 % for the B_c semileptonic decays.

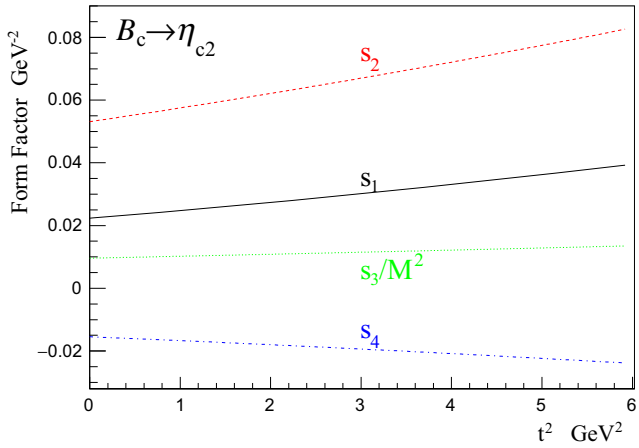

(a) Form factors of $B_c \to \eta_{c2}(1^1D_2)$.

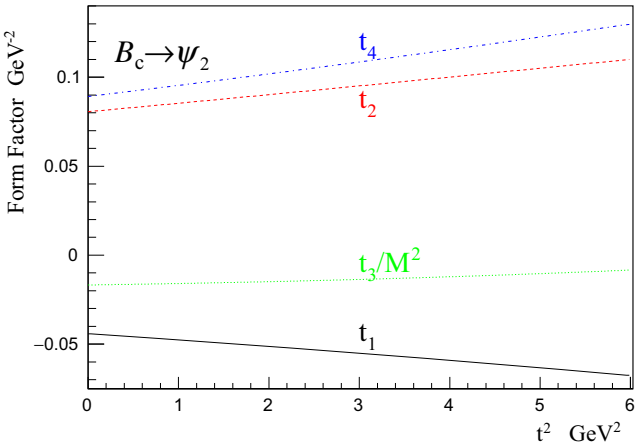

(b) Form factors of $B_c \to \psi_2(1^3D_2)$.

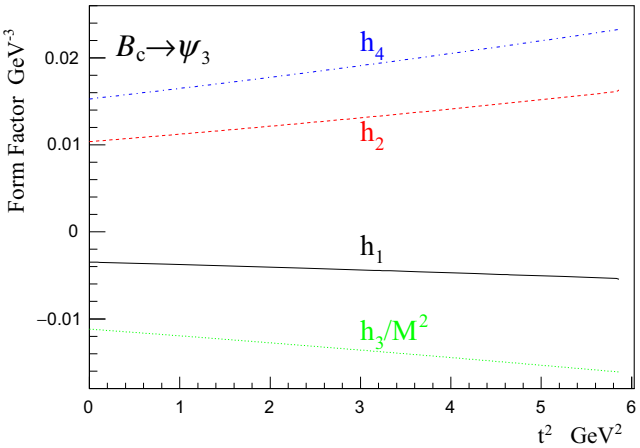

(c) Form factors of $B_c \to \psi_3(1^3D_3)$.

Fig. 3 Form factors for $B_c \to \eta_{c2}$, ψ_2 and ψ_3. $t^2 = (P - P_F)^2$ and t denotes the transferred momentum. We have divided s_3, t_3, and h_3 by M^2 to keep their dimensions consistent with others'

Table 1 Branching ratios of B_c semileptonic decays. The uncertainties here are determined by varying the model parameters by ±5 % and then finding the maximum deviation

Channels	Ours	Ref. [8]	Ref. [9]	Ref. [13]
$B_c^- \to \eta_{c2} e \bar{\nu}$	$5.9^{-0.8}_{+1.0} \times 10^{-4}$	–	–	–
$B_c^- \to \eta_{c2} \mu \bar{\nu}$	$5.8^{-0.8}_{+1.0} \times 10^{-4}$	–	–	–
$B_c^- \to \eta_{c2} \tau \bar{\nu}$	$4.9^{-0.8}_{+1.0} \times 10^{-6}$	–	–	–
$B_c^- \to \psi_2 e \bar{\nu}$	$1.5^{-0.2}_{+0.3} \times 10^{-4}$	8.9×10^{-5}	6.6×10^{-5}	$4.3^{-0.5} \times 10^{-5}$
$B_c^- \to \psi_2 \mu \bar{\nu}$	$1.5^{-0.2}_{+0.3} \times 10^{-4}$	–	–	–
$B_c^- \to \psi_2 \tau \bar{\nu}$	$2.3^{-0.4}_{+0.5} \times 10^{-6}$	2.1×10^{-6}	9.9×10^{-7}	$8.3^{-1.0} \times 10^{-7}$
$B_c^- \to \psi_3 e \bar{\nu}$	$3.5^{-0.6}_{+0.8} \times 10^{-4}$	–	–	–
$B_c^- \to \psi_3 \mu \bar{\nu}$	$3.4^{-0.6}_{+0.7} \times 10^{-4}$	–	–	–
$B_c^- \to \psi_3 \tau \bar{\nu}$	$2.3^{-0.5}_{+0.6} \times 10^{-6}$	–	–	–

Our result for the branching ratio of the channel $B_c \to \psi_2 e \bar{\nu}_e$ is 1.5×10^{-4}, which is larger than those of Refs. [8,9] and Ref. [13]. For the channel with τ as the final lepton, our result is very close to that in Ref. [8], but more than two times larger than those of Refs. [9,13]. The method used in Ref. [13] is non-relativistic constituent quark model.

Both Ref. [8] and Ref. [9] used the same relativistic constituent quark model whose framework is relativistic covariant while the wave functions of mesons are assumed to be the Gaussian type. As to our method, although the instantaneous approximation causes the lost of relativistic covariant, the wave functions are more reasonable. For the η_{c2} and ψ_3 cases, we get $\mathcal{B}(B_c \to \eta_{c2} e\bar{\nu}_e) = 5.9 \times 10^{-4}$ and $\mathcal{B}(B_c \to \psi_3 e\bar{\nu}_e) = 3.5 \times 10^{-4}$, which are larger than that of the ψ_2 case. From this point, the former two channels have more possibilities to be detected in the future experiments.

As an experimentally interested quantity, the numerical results for the forward–backward asymmetry A_{FB} are listed in Table 2. For the $B_c \to \psi_2 \ell\bar{\nu}$ channel, our results are consistent with those in Ref. [13] but larger than those in Ref. [8]. We notice that for all the cases when $\ell = e$, μ, and τ, $A_{FB}(\psi_2)$ is negative. For the $B_c \to \eta_{c2}\ell\bar{\nu}$ channel, when $\ell = e$, $A_{FB}(\eta_{c2})$ is negative, while for the $B_c \to \psi_3\ell\bar{\nu}$ channel, when $\ell = e$ and μ, $A_{FB}(\psi_3)$ is negative. For the absolute value of this quantity, when $\ell = e$, we have $A_{FB}(\eta_{c2}) < A_{FB}(\psi_3) < A_{FB}(\psi_2)$.

Table 2 A_{FB} of B_c semileptonic decays

Channels	Ours	Ref. [8]	Ref. [13]
$B_c^- \to \eta_{c2} e\bar{\nu}$	−0.020	–	–
$B_c^- \to \eta_{c2}\mu\bar{\nu}$	0.011	–	–
$B_c^- \to \eta_{c2}\tau\bar{\nu}$	0.35	–	–
$B_c^- \to \psi_2 e\bar{\nu}$	−0.56	−0.21	−0.59
$B_c^- \to \psi_2\mu\bar{\nu}$	−0.56	–	−0.59
$B_c^- \to \psi_2\tau\bar{\nu}$	−0.37	−0.21	−0.42
$B_c^- \to \psi_3 e\bar{\nu}$	−0.11	–	–
$B_c^- \to \psi_3\mu\bar{\nu}$	−0.090	–	–
$B_c^- \to \psi_3\tau\bar{\nu}$	0.10	–	–

For the sake of completeness, we also plot Figs. 4 and 5 to show the spectra of decay widths varying along $\cos\theta$ and 3-momentum $|\boldsymbol{p}_\ell|$ of the charged lepton, respectively. Here we do not give the result of μ mode which is almost the same as that of $\ell = e$. For the angular distribution in Fig. 4, we can see when $\ell = e$, $\mathrm{d}\Gamma/(\Gamma \mathrm{d}\cos\theta)$ decreases monotonously for ψ_2 when $\cos\theta$ varies from -1 to 1, but reaches the maximum value for η_{c2} and ψ_3 in the vicinity of 0. When $\ell = \tau$, all the three distributions are monotonic functions (for η_{c2} and ψ_3, the angular spectra are increasing functions, while for ψ_2, it is a decreasing function). As to the momentum distribution (see Fig. 5), one can see the results of η_{c2} and ψ_3 are more symmetrical than that of ψ_2, especially for $\ell = e$. These results will be useful to the future experiments.

4.2 Results of nonleptonic decays and uncertainties estimation

The nonleptonic decay widths of B_c to D-wave charmonia are listed in Table 3. In the calculation, the decay constants of the charged mesons are [6,9]

$$f_\pi = 130.4\ \mathrm{MeV}, \quad f_K = 156.2\ \mathrm{MeV}, \quad f_\rho = 210\ \mathrm{MeV}, \quad f_{K^*} = 217\ \mathrm{MeV}.$$

The factorization method is used and the decay widths are expressed with general Wilson coefficient a_1. In this paper, to calculate the branching ratios of nonleptonic decays we choose $a_1 = 1.14$ [9].

The branching ratios of the nonleptonic decays are listed in Tables 4 and 5. For the channels with ψ_2 as the final charmonium, when the light meson is pseudoscalar, the branch-

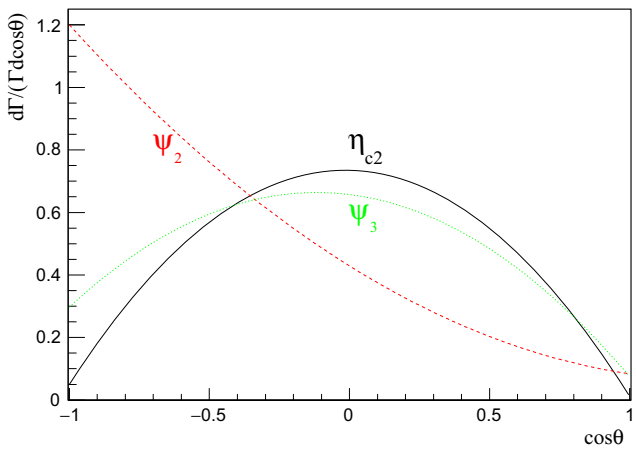

(a) Angular spectrum for decay to e mode.

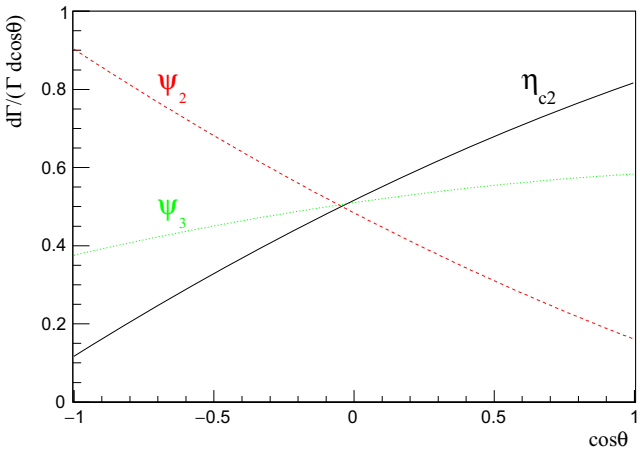

(b) Angular spectrum for decay to τ mode.

Fig. 4 The spectra of relative width vs. $\cos\theta$ in B_c semileptonic decays into D-wave charmonia. θ is the angle between charged lepton ℓ and final $c\bar{c}$ system in the rest frame of $\ell\bar{\nu}$

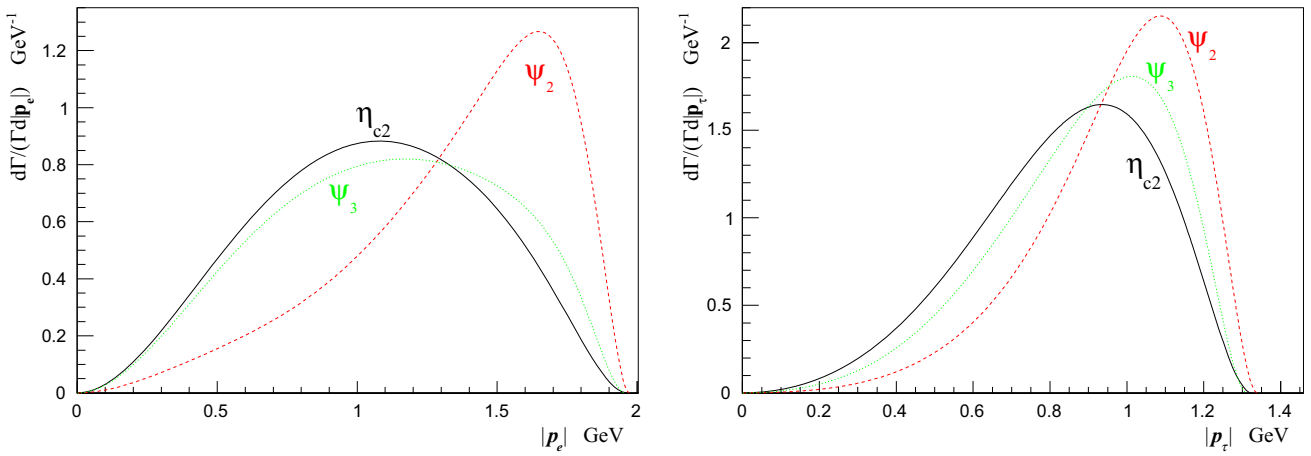

(a) Momentum spectrum for decay to e mode. **(b)** Momentum spectrum for decay to τ mode.

Fig. 5 The spectra of relative width vs. charged leptons 3-momentum in B_c semileptonic decays into D wave charmonia. $|\boldsymbol{p}_e|$ and $|\boldsymbol{p}_\tau|$ are the 3-momentum amplitudes of e and τ, respectively

Table 3 Nonleptonic decays width for B_c^- to η_{c2}, ψ_2 and ψ_3 with general Wilson coefficient a_1

Channels	Width	Channels	Width	Channels	$\times a_1^2$ (GeV) Width
$B_c^- \to \psi_2 \pi^-$	$1.2^{-0.1}_{+0.1} \times 10^{-17}$	$B_c^- \to \eta_{c2} \pi^-$	$4.4^{-0.6}_{+0.7} \times 10^{-16}$	$B_c^- \to \psi_3 \pi^-$	$1.9^{-0.3}_{+0.4} \times 10^{-16}$
$B_c^- \to \psi_2 K^-$	$8.3^{-0.7}_{+0.7} \times 10^{-19}$	$B_c^- \to \eta_{c2} K^-$	$3.2^{-0.4}_{+0.5} \times 10^{-17}$	$B_c^- \to \psi_3 K^-$	$1.3^{-0.2}_{+0.3} \times 10^{-17}$
$B_c^- \to \psi_2 \rho^-$	$1.1^{-0.1}_{+0.2} \times 10^{-16}$	$B_c^- \to \eta_{c2} \rho^-$	$9.1^{-1.0}_{+2.0} \times 10^{-16}$	$B_c^- \to \psi_3 \rho^-$	$4.6^{-0.7}_{+0.9} \times 10^{-16}$
$B_c^- \to \psi_2 K^{*-}$	$7.1^{-0.9}_{+1.0} \times 10^{-18}$	$B_c^- \to \eta_{c2} K^{*-}$	$4.8^{-0.7}_{+0.8} \times 10^{-17}$	$B_c^- \to \psi_3 K^{*-}$	$2.5^{-0.4}_{+0.5} \times 10^{-17}$

Table 4 Branching ratios of nonleptonic decays for B_c^- to ψ_2. $a_1 = 1.14$ and $\tau_{B_c} = 0.452 \times 10^{-12}$ s. The first uncertainties are from varying the model parameters by ± 5 % then finding the maximum deviation. The second uncertainties are from the calculations of the Wilson coefficient $a_1 = c_1 + \frac{1}{N_c} c_2$, where we change N_c from 2 to $+\infty$ to estimate the non-factorizable contributions

Channels	BR	Ref. [9]	Ref. [13]
$B_c^- \to \psi_2 \pi^-$	$1.0^{-0.1-0.2}_{+0.1+0.4} \times 10^{-5}$	1.7×10^{-5}	$4.1^{-0.02}_{+0.03} \times 10^{-7}$
$B_c^- \to \psi_2 K^-$	$7.4^{-0.6-1.4}_{+0.6+3.1} \times 10^{-7}$	1.2×10^{-6}	$3.1^{-0.2}_{+0.2} \times 10^{-8}$
$B_c^- \to \psi_2 \rho^-$	$9.6^{-1.0-1.7}_{+1.0+4.0} \times 10^{-5}$	5.5×10^{-5}	$2.0^{-0.3} \times 10^{-5}$
$B_c^- \to \psi_2 K^{*-}$	$6.4^{-0.8-1.2}_{+1.0+2.7} \times 10^{-6}$	3.2×10^{-6}	$1.4^{-0.2} \times 10^{-6}$

ing ratio is smaller than that of Ref. [9] but about 20 times larger than that of Ref. [13], while for the channels with vector charged mesons, the branching ratios are about 2 times and 5 times larger than those of Refs. [9,13], respectively. Within all nonleptonic channels, those with ρ as the charged meson have the largest branching ratios, which have more possibilities to be discovered by the future experiments.

In order to estimate the systematic theoretical uncertainties for nonleptonic decays, we vary the parameters of Cornell potential model by ± 5 % and then scanning the parameter space to find the maximum deviation. From our results (see Table 3), the deviations of nonleptonic B_c decays amount to 5−20 %.

In the method of the factorization approximation, the number of colors N_c, which appeared in the calculation of the Wilson coefficient $a_1 = c_1 + \frac{1}{N_c} c_2$, is a parameter to be determined by experimental data. To estimate the systematic uncertainties from the non-factorizable contributions, we change the value of N_c within the range $[2, +\infty]$, and then we calculate the maximum deviation to the central values where $N_c = 3$ and $a_1 = 1.14$ are used. In our calculations, these uncertainties can amount to about 15% ∼ 40% in the nonleptonic decays of B_c to D-wave charmonia, which are listed as the second uncertainties in the results of the branching ratios in Tables 4 and 5.

Table 5 Branching ratios of nonleptonic decays for B_c^- to η_{c2} and ψ_3. $a_1 = 1.14$ and $\tau_{B_c} = 0.452 \times 10^{-12}$ s. See the caption of Table 4 for further explanations

Channels	BR	Channels	BR
$B_c^- \to \eta_{c2}\pi^-$	$3.9^{-0.5-0.7}_{+0.6+1.6} \times 10^{-4}$	$B_c^- \to \psi_3\pi^-$	$1.7^{-0.3-0.3}_{+0.3+0.7} \times 10^{-4}$
$B_c^- \to \eta_{c2}K^-$	$2.8^{-0.4-0.5}_{+0.5+1.2} \times 10^{-5}$	$B_c^- \to \psi_3 K^-$	$1.2^{-0.2-0.2}_{+0.2+0.5} \times 10^{-5}$
$B_c^- \to \eta_{c2}\rho^-$	$8.1^{-1.0-1.5}_{+1.0+3.4} \times 10^{-4}$	$B_c^- \to \psi_3\rho^-$	$4.1^{-0.7-0.7}_{+0.8+1.7} \times 10^{-4}$
$B_c^- \to \eta_{c2}K^{*-}$	$4.3^{-0.6-0.8}_{+0.7+1.8} \times 10^{-5}$	$B_c^- \to \psi_3 K^{*-}$	$2.3^{-0.4-0.4}_{+0.5+0.9} \times 10^{-5}$

5 Summary

In this work we calculated semileptonic and nonleptonic decays of B_c into the D-wave charmonia, namely, $\eta_{c2}(1^1D_2)$, $\psi_2(1^3D_2)$, and $\psi_3(1^3D_3)$, whose decay widths are expected to be narrow. The results show that for the semileptonic channels with the charged lepton to be e or μ, the branching ratios are of the order of 10^{-4}. For the nonleptonic decay channels, the largest branching ratio is also of the order of 10^{-4}. These results can be useful for future experiments to study the D-wave charmonia.

Acknowledgments This work was supported in part by the National Natural Science Foundation of China (NSFC) under Grant Nos. 11405037, 11575048 and 11505039, and in part by PIRS of HIT Nos. T201405, A201409, and B201506. We thank Wei Feng of Bordeaux INP for her thorough proofreading of the manuscript.

Appendix A: Expressions for the N_i in the hadronic tensor $H_{\mu\nu}$

The hadronic tensors N_i for the B_c to $^1D_2$ $c\bar{c}$ states are

$$N_1 = \frac{2M^4 p_F^4 s_1^2}{3M_F^4} - \frac{4M^2 p_F^2 s_1 s_3}{3M_F^2} - \frac{1}{2}M^2 p_F^2 s_4^2 + \frac{s_3^2}{6}, \quad (A.1)$$

$$N_2 = \frac{2E_F M^3 p_F^2 s_1 s_3}{3M_F^4} + \frac{E_F M^3 p_F^2 s_4^2}{2M_F^2} - \frac{E_F M s_3^2}{6M_F^2} + \frac{2M^4 p_F^4 s_1 s_2}{3M_F^4} - \frac{2M^2 p_F^2 s_2 s_3}{3M_F^2}, \quad (A.2)$$

$$N_4 = \frac{4E_F M^3 p_F^2 s_2 s_3}{3M_F^4} + \frac{2M^4 p_F^4 s_2^2}{3M_F^4} - \frac{M^4 p_F^2 s_4^2}{2M_F^2} + \frac{M^2 s_3^2 (M_F^2 + 4p_F^2)}{6M_F^4}, \quad (A.3)$$

$$N_5 = -\frac{M^4 p_F^4 s_4^2}{2M_F^2} - \frac{M^2 p_F^2 s_3^2}{2M_F^2}, \quad (A.4)$$

$$N_6 = -\frac{M^2 p_F^2 s_3 s_4}{M_F^2}. \quad (A.5)$$

For the B_c to $^3D_2$ state the relations between N_i ($i = 1, 2, 4, 5, 6$) and form factors t_j ($j = 1, 2, 3, 4$) are the same as the $^1D_2$ state, just s_j are replaced with t_j.

The hadronic tensor N_i ($i = 1, 2, 4, 5, 6$) for B_c to $^3D_3$ charmonium are expressed with corresponding form factors h_j ($j = 1, 2, 3, 4$) as

$$N_1 = \frac{2M^6 p_F^6 h_1^2}{5M_F^6} - \frac{4M^4 p_F^4 h_1 h_3}{5M_F^4} - \frac{4M^4 p_F^4 h_4^2}{15M_F^2} + \frac{2M^2 p_F^2 h_3^2}{15M_F^2}, \quad (A.6)$$

$$N_2 = \frac{2E_F M^5 p_F^4 h_1 h_3}{5M_F^6} + \frac{4E_F M^5 p_F^4 h_4^2}{15M_F^4} - \frac{2E_F M^3 p_F^2 h_3^2}{15M_F^4} + \frac{2M^6 p_F^6 h_1 h_2}{5M_F^6} - \frac{2M^4 p_F^4 h_2 h_3}{5M_F^4}, \quad (A.7)$$

$$N_4 = \frac{4E_F M^5 p_F^4 h_2 h_3}{5M_F^6} + \frac{2M^6 p_F^6 h_2^2}{5M_F^6} - \frac{4M^6 p_F^4 h_4^2}{15M_F^4} + \frac{2M^4 p_F^2 h_3^2 (M_F^2 + 3p_F^2)}{15M_F^6}, \quad (A.8)$$

$$N_5 = -\frac{4M^6 p_F^6 h_4^2}{15M_F^4} - \frac{4M^4 p_F^4 h_3^2}{15M_F^4}, \quad (A.9)$$

$$N_6 = -\frac{8M^4 p_F^4 h_3 h_4}{15M_F^4}. \quad (A.10)$$

Appendix B: Expressions for x_i in form factors s_i

The expressions for the x_i ($i = 1, 2, \ldots, 11$) in Eq. (49) are

$$x_1 = -\frac{4\alpha_2'^2 E_F^2}{M^4 M_F^2}(\alpha_2' A_1 B_4 E_F^2 M + A_1 B_1 M M_F^2 + A_3 B_2 M_F \boldsymbol{P}_F \cdot \boldsymbol{q} + \alpha_2' A_4 B_4 E_F \boldsymbol{P}_F \cdot \boldsymbol{q}). \quad (B.1)$$

$$x_2 = +\frac{4\alpha_2'^2 E_F^2}{M^3 M_F^2}(\alpha_2' A_1 B_4 E_F M - A_2 B_2 M M_F - A_4 B_4 \boldsymbol{q}^2). \quad (B.2)$$

$$x_3 = +\frac{4\alpha_2'^2 E_F^2}{M^3 M_F^2}(A_1 B_4 E_F M - A_3 B_2 E_F M_F$$

$$+A_4B_1M_F^2+A_4B_4\boldsymbol{P}_F\cdot\boldsymbol{q}). \tag{B.3}$$

$$x_4=+\frac{8\alpha_2'E_F}{M^3M_F^2}(\alpha_2'A_1B_4E_F^2M+A_1B_1MM_F^2 +A_3B_2M_F\boldsymbol{P}_F\cdot\boldsymbol{q}+\alpha_2'A_4B_4E_F\boldsymbol{P}_F\cdot\boldsymbol{q}). \tag{B.4}$$

$$x_5=-\frac{8\alpha_2'E_F}{M^2M_F^2}(\alpha_2'A_1B_4E_FM-A_2B_2MM_F-A_4B_4\boldsymbol{q}^2). \tag{B.5}$$

$$x_6=-\frac{8\alpha_2'E_F}{M^2M_F^2}(A_1B_4E_FM-A_3B_2E_FM_F +A_4B_1M_F^2+A_4B_4\boldsymbol{P}_F\cdot\boldsymbol{q}). \tag{B.6}$$

$$x_7=-\frac{4}{M^2M_F^2}(\alpha_2'A_1B_4E_F^2M+A_1B_1MM_F^2 +A_3B_2M_F\boldsymbol{P}_F\cdot\boldsymbol{q}+\alpha_2'A_4B_4E_F\boldsymbol{P}_F\cdot\boldsymbol{q}). \tag{B.7}$$

$$x_8=+\frac{4}{MM_F^2}(\alpha_2'A_1B_4E_FM-A_2B_2MM_F-A_4B_4\boldsymbol{q}^2). \tag{B.8}$$

$$x_9=+\frac{4}{MM_F^2}(A_1B_4E_FM-A_3B_2E_FM_F+A_4B_1M_F^2 +A_4B_4\boldsymbol{P}_F\cdot\boldsymbol{q}). \tag{B.9}$$

$$x_{10}=-\frac{8\alpha_2'E_F}{M^3M_F^2}(-A_1B_4M+A_3B_2M_F+\alpha_2'A_4B_4E_F). \tag{B.10}$$

$$x_{11}=+\frac{4}{M^2M_F^2}(-A_1B_4M+A_3B_2M_F+\alpha_2'A_4B_4E_F), \tag{B.11}$$

where $\alpha_2'=\frac{1}{2}$.

Appendix C: BS positive wave function for the $^3D_2$ and $^3D_3$ states

The wave function for $^3D_2(2^{--})$ $c\bar{c}$ can be written as [34]

$$\varphi^{++}(^3D_2)=\mathrm{i}\epsilon_{\mu\nu\alpha\beta}\frac{P_F^\nu}{M_F}q_\perp'^\alpha e^{\beta\delta}q'_{\perp\delta}\gamma^\mu \times\left[i_1+i_2\frac{\not{P}_F}{M_F}+i_4\frac{\not{P}_F\not{q}'_\perp}{M_F^2}\right]. \tag{C.1}$$

i_1, i_2 and i_4 are defined as

$$i_1=\frac{1}{2}\left[I_1-\frac{\omega_c}{m_c}I_2\right],\quad i_2=\frac{1}{2}\left[I_2-\frac{m_c}{\omega_c}I_1\right],\quad i_4=-\frac{M_F}{\omega_c}i_1. \tag{C.2}$$

I_1 and I_2 are functions of $q_\perp'^2$.

The positive part of the wave function of the $^3D_3(3^{--})$ state has the form [34]

$$\varphi^{++}(^3D_3)=e_{\mu\nu\alpha}q_\perp'^\nu q_\perp'^\alpha \times\left[q_\perp'^\mu\left(u_1+u_3\frac{\not{q}'_\perp}{M_F}+u_4\frac{\not{P}_F\not{q}_\perp}{M_F^2}\right)+\gamma^\mu(u_5M_F+u_6\not{P}_F) +u_8\frac{(\gamma^\mu\not{P}_F\not{q}'_\perp+\not{P}_F\not{q}_\perp'^\mu)}{M_F}\right], \tag{C.3}$$

where u_i $(i=1,3,4,5,6,8)$ are expressed as

$$u_1=\frac{\omega_c(q_\perp^2U_3+M_F^2U_5)+m_c(q_\perp^2U_4-M_F^2U_6)}{2M_Fm_c\omega_c},$$
$$u_3=\frac{1}{2}\left[U_3+\frac{m_c}{\omega_c}U_4-\frac{M_F^2}{m_c\omega_c}U_6\right],$$
$$u_4=\frac{1}{2}\left[U_4+\frac{\omega_c}{m_c}U_3-\frac{M_F^2}{m_c\omega_c}U_5\right],$$
$$u_5=\frac{1}{2}\left[U_5-\frac{\omega_c}{m_c}U_6\right],$$
$$u_6=\frac{1}{2}\left[U_6-\frac{m_c}{\omega_c}U_5\right],$$
$$u_8=-\frac{M_F}{\omega_c}u_5. \tag{C.4}$$

In the above expressions U_3 , U_4, U_5, and U_6 are functions of $q_\perp'^2$, which could be determined numerically by solving the full Salpeter equation.

References

1. V. Bhardwaj et al. (Belle Collaboration), Phys. Rev. Lett. **111**, 032001 (2013). doi:10.1103/PhysRevLett.111.032001
2. M. Ablikim et al. (BESIII Collaboration), Phys. Rev. Lett. **115**, 011803 (2015). doi:10.1103/PhysRevLett.115.011803
3. S. Godfrey, N. Isgur, Phys. Rev. D **32**, 189 (1985). doi:10.1103/PhysRevD.32.189
4. D. Ebert, R.N. Faustov, V.O. Galkin, Phys. Rev. D **67**, 014027 (2003). doi:10.1103/PhysRevD.67.014027
5. F. Abe et al. (CDF Collaboration), Phys. Rev. Lett. **81**, 2432 (1998). doi:10.1103/PhysRevLett.81.2432
6. K.A. Olive et al. (Particle Data Group), Chin. Phys. C **38**, 090001 (2014). doi:10.1088/1674-1137/38/9/090001
7. C.-H. Chang, Y.-Q. Chen, Phys. Rev. D **49**, 3399 (1994). doi:10.1103/PhysRevD.49.3399
8. M.A. Ivanov, J.G. Körner, P. Santorelli, Phys. Rev. D **71**, 094006 (2005). doi:10.1103/PhysRevD.71.094006
9. M.A. Ivanov, J.G. Körner, P. Santorelli, Phys. Rev. D **73**, 054024 (2006). doi:10.1103/PhysRevD.73.054024
10. A.A. El-Hady, J.H. Muñoz, J.P. Vary, Phys. Rev. D **62**, 014019 (2000). doi:10.1103/PhysRevD.62.014019
11. M.A. Ivanov, J.G. Körner, P. Santorelli, Phys. Rev. D **63**, 074010 (2001). doi:10.1103/PhysRevD.63.074010
12. D. Ebert, R.N. Faustov, V.O. Galkin, Phys. Rev. D **68**, 094020 (2003). doi:10.1103/PhysRevD.68.094020
13. E. Hernández, J. Nieves, J.M. Verde-Velasco, Phys. Rev. D **74**, 074008 (2006). doi:10.1103/PhysRevD.74.074008
14. V.V. Kiselev, O.N. Pakhomova, V.A. Saleev, J. Phys. G: Nucl. Part. Phys. **28**, 595 (2002). http://stacks.iop.org/JPhysG/28/595

15. J.F. Sun, G.F. Xue, Y.L. Yang, G.R. Lu, D.S. Du, Phys. Rev. D **77**, 074013 (2008). doi:10.1103/PhysRevD.77.074013
16. V.V. Kiselev, A.K. Likhoded, A.I. Onishchenko, Nucl. Phys. B **569**, 473 (2000). doi:10.1103/Nucl.Phys.B.569.473
17. T. Huang, F. Zuo, Eur. Phys. J. C **51**, 833 (2007). doi:10.1140/epjc/s10052-007-0333-4
18. J.F. Sun, D.S. Du, Y.L. Yang, Eur. Phys. J. C **60**, 107 (2009). doi:10.1140/epjc/s10052-009-0872-y
19. Z.-J. Xiao, X. Liu, Chin. Sci. Bull. **59**, 3748 (2014). doi:10.1103/Chin.Sci.Bull.59.3748
20. Z. Rui, Z.-T. Zou, Phys. Rev. D **90**, 114030 (2014). doi:10.1103/PhysRevD.90.114030
21. Z. Rui, W.-F. Wang, G.-X. Wang, L.-H. Song, C.-D. Lü, Eur. Phys. J. C **75**, 293 (2015). doi:10.1140/epjc/s10052-015-3528-0
22. C.-F. Qiao, R.-L. Zhu, Phys. Rev. D **87**, 014009 (2013). doi:10.1103/PhysRevD.87.014009
23. C.-F. Qiao, P. Sun, D. Yang, R.-L. Zhu, Phys. Rev. D **89**, 034008 (2014). doi:10.1103/PhysRevD.89.034008
24. C.-H. Chang, Y.-Q. Chen, G.-L. Wang, H.-S. Zong, Phys. Rev. D **65**, 014017 (2001). doi:10.1103/PhysRevD.65.014017
25. Y.M. Wang, C.D. Lü, Phys. Rev. D **77**, 054003 (2008). doi:10.1103/PhysRevD.77.054003
26. X.X. Wang, W. Wang, C.D. Lü, Phys. Rev. D **79**, 114018 (2009). doi:10.1103/PhysRevD.79.114018
27. D. Ebert, R.N. Faustov, V.O. Galkin, Phys. Rev. D **82**, 034019 (2010). doi:10.1103/PhysRevD.82.034019
28. Z.-H. Wang, G.-L. Wang, C.-H. Chang, J. Phys. G: Nucl. Part. Phys. **39**, 015009 (2012). doi:10.1088/0954-3899/39/1/015009
29. E. Salpeter, H. Bethe, Phys. Rev. **84**, 1232 (1951). doi:10.1103/PhysRev.84.1232
30. E.E. Salpeter, Phys. Rev. **87**, 328 (1952). doi:10.1103/PhysRev.87.328
31. G.-L. Wang, Phys. Lett. B **633**, 492 (2006). doi:10.1016/j.physletb.2005.12.005
32. G.-L. Wang, Phys. Lett. B **674**, 172 (2009). doi:10.1016/j.physletb.2009.03.030
33. T. Wang, G.-L. Wang, W.-L. Ju, Y. Jiang, JHEP **03**, 110 (2013). doi:10.1007/JHEP03(2013)110
34. T. Wang, H.-F. Fu, Y. Jiang, Q. Li, G.-L. Wang, arXiv:1601.01047 [hep-ph]
35. D. Fakirov, B. Stech, Nucl. Phys. B **133**, 315 (1978). doi:10.1016/0550-3213(78)90306-1
36. N. Cabibbo, L. Maiani, Phys. Lett. B **73**, 418 (1978). doi:10.1016/0370-2693(78)90754-2
37. G. Buchalla, A.J. Buras, M.E. Lautenbacher, Rev. Mod. Phys. **68**, 1125 (1996). doi:10.1103/RevModPhys.68.1125
38. R.N. Faustov, V.O. Galkin, Phys. Rev. D **87**, 034033 (2013). doi:10.1103/PhysRevD.87.034033
39. M.J. Dugan, B. Grinstein, Phys. Lett. B **255**, 583 (1991). doi:10.1016/0370-2693(91)90271-Q
40. W.-L. Ju, G.-L. Wang, H.-F. Fu, Z.-H. Wang, Y. Li, JHEP **09**, 171 (2015). doi:10.1007/JHEP09(2015)171
41. C.S. Kim, G.-L. Wang, Phys. Lett. B **584**, 285 (2004). doi:10.1016/j.physletb.2004.01.058
42. T. Wang, G.-L. Wang, Y. Jiang, W.-L. Ju, J. Phys. G **40**, 035003 (2013). doi:10.1088/0954-3899/40/3/035003
43. S. Mandelstam, Proc. Roy. Soc. A **233**, 248 (1955). doi:10.1098/rspa.1955.0261
44. B. Durand, L. Durand, Phys. Rev. D **25**, 2312 (1982). doi:10.1103/PhysRevD.25.2312
45. C.-H. Chang, G.-L. Wang, Sci. China Phys. Mech. Astron. **53**, 11 (2005). doi:10.1007/s11433-010-4156-1
46. L. Bergström, H. Grotch, R.W. Robinett, Phys. Rev. D. **43**, 7 (1991). doi:10.1103/PhysRevD.43.2157
47. C.-F. Qiao, F. Yuan, K.-T. Chao, Phys. Rev. D **55**, 7 (1997). doi:10.1103/PhysRevD.55.4001
48. B.-Q. Li, K.-T. Chao, Phys. Rev. D **79**, 094004 (2009). doi:10.1103/PhysRevD.79.094004
49. T. Barnes, S. Godfrey, E.S. Swanson, Phys. Rev. D **72**, 054026 (2005). doi:10.1103/PhysRevD.72.054026
50. E.J. Eichten, K. Lane, C. Quigg, Phys. Rev. D **73**, 014014 (2006). doi:10.1103/PhysRevD.73.014014